Daytime aerosol optical depth above low-level clouds is similar to that in adjacent clear skies at the same heights: airborne observation above the southeast Atlantic

Yohei Shinozuka[1,2], Meloë S. Kacenelenbogen[2], Sharon P. Burton[3], Steven G. Howell[4], Paquita Zuidema[5], Richard A. Ferrare[3], Samuel E. LeBlanc[2,6], Kristina Pistone[2,6], Stephen Broccardo[1,2], Jens Redemann[7], K. Sebastian Schmidt[8], Sabrina P. Cochrane[8,9], Marta Fenn[3,10], Steffen Freitag[4], Amie Dobracki[4,5], Michal Segal-Rosenheimer[2,6,11], Connor J. Flynn[7]

[1] Universities Space Research Association, Columbia, Maryland, USA
[2] NASA Ames Research Center, Moffett Field, California, USA
[3] NASA Langley Research Center, Hampton, Virginia, USA
[4] University of Hawaii at Manoa, Honolulu, Hawaii, USA
[5] University of Miami, Miami, Florida, USA
[6] Bay Area Environmental Research Institute, Moffett Field, California, USA
[7] University of Oklahoma, Norman, Oklahoma, USA
[8] University of Colorado, Boulder, Colorado, USA
[9] Laboratory for Atmospheric and Space Physics, Boulder, Colorado, USA
[10] Science Systems and Applications, Inc, Hampton, VA, USA
[11] Department of Geophysics, Porter School of the Environment and Earth Sciences, Tel-Aviv University, Tel-Aviv, Israel

Correspondence to: Y. Shinozuka (Yohei.Shinozuka@nasa.gov)

23 **Abstract**

24 To help satellite retrieval of aerosols and studies of their radiative effects, we demonstrate

25 that daytime aerosol optical depth over low-level clouds is similar to that in neighboring clear skies

26 at the same heights. Based on recent airborne lidar and sunphotometer observations above the

27 southeast Atlantic, the mean AOD difference at 532 nm is between 0 and -0.01, when comparing

28 the cloudy and clear sides, each up to 20 km wide, of cloud edges. The difference is not statistically

29 significant according to a paired t-test. Systematic differences in the wavelength dependence of

30 AOD and in situ single scattering albedo are also minuscule. These results hold regardless of the

31 vertical distance between cloud top and aerosol layer bottom. AOD aggregated over ~2° grid boxes

32 for each of September 2016, August 2017 and October 2018 also shows little correlation with the

33 presence of low-level clouds. We posit that a satellite retrieval artifact is entirely responsible for a

34 previous finding of generally smaller AOD over clouds (Chung et al., 2016), at least for the region

35 and time of our study. Our results also suggest that the same values can be assumed for the

36 intensive properties of free-tropospheric biomass-burning aerosol regardless of whether clouds are

37 present below.

38 **1.   Introduction**

39 A significant amount of atmospheric particles are transported above liquid water clouds on

40 the global scale (Waquet et al., 2013). Aerosols above clouds (AAC) may influence the climate in

41 three ways: their light absorption may be amplified by cloud reflection; the heating of the

42 atmosphere due to the absorption may stabilize the atmosphere; and the particles may eventually

43 subside, enter the underlying clouds and alter their properties. Estimates of the direct aerosol

44 radiative effect alone see large inter-model spread for areas with large aerosol optical depth (AOD)

45 over widespread clouds (Stier et al., 2013; Zuidema et al., 2016).

46 Since AAC are difficult to see from the ground or a ship, previous studies have relied on

47 satellite observations (see Table 1 and 2 of Kacenelenbogen et al. (2019)). Among them is Chung

48 et al. (2016), which used the level 2 products of the Cloud-Aerosol Lidar with Orthogonal

49 Polarization (CALIOP) (Winker et al., 2009) to calculate the AOD above the maximum low-cloud-

50 top-height in each grid cell in clear sky as well as the AOD above low clouds on a global $2^\circ \times 5^\circ$

51 latitude–longitude grid. Their results indicate that daytime 532 nm AOD above low clouds is

52 generally lower than that in clear sky at the same heights. The difference is up to 0.04 over the
53 southeastern Atlantic Ocean (see their Fig. 2).

54   As Chung et al. (2016) point out, it is conceivable that aerosol amounts over cloud can be
55 different from those in nearby clear sky. There are two sets of potential reasons. The first concerns
56 the effects of meteorology. Large-scale circulation patterns paired with solar reflection from clouds
57 on aerosols could modify the horizontal and vertical extent of aerosols, aerosol concentration and
58 chemical composition. For example, the properties of hygroscopic aerosols might vary if the
59 relative humidity in clear skies is somehow higher than above clouds. The second set of reasons
60 pertain to the case of aerosols in close proximity to clouds. That proximity has been variously
61 defined, for example less than 100 m in the vertical direction (Costantino and Bréon, 2013) and
62 less than 20 km in the horizontal direction (Várnai and Marshak, 2018). Chung et al. (2016) note
63 that aerosols were shown to influence underlying cloud by indirect effects and semidirect effects
64 (Costantino and Bréon, 2010, 2013; Johnson et al., 2004; Wilcox, 2010) and that these aerosol–
65 cloud interactions and possibly more might somehow affect the aerosol amount over cloud.

66   Chung et al. (2016) raise a bias in the CALIOP standard retrieval as another possible
67 explanation. The retrieval algorithm confines itself to distinct aerosol layers whose signals are high
68 enough compared to detector noise. The detection threshold varies with the atmospheric features
69 (e.g., aerosols, high altitude cirrus or boundary layer clouds), the horizontal averaging required by
70 CALIOP for detection and, importantly, the background lighting conditions (see Fig. 4 of Winker
71 et al. (2009)). If the signal-to-noise (S/N) ratio of a layer is not high enough, no extinction is
72 reported for the portion of the aerosol profile; summing up the extinction produces a low-biased
73 AOD. Because the upward sunlight reflection adds to the background noise, the AOD
74 underestimate is likely more pronounced above clouds than in clear skies. Chung et al. (2016) state
75 that their results "might simply be a result of systematic differences between the detection
76 thresholds in clear sky and above low bright clouds." Layer detection and other sources of
77 uncertainty in the CALIPSO standard algorithm are also discussed by Kacenelenbogen et al.
78 (2014) and Liu et al. (2015).

79   The subject warrants further investigation, given the importance of AAC on climate. An
80 airborne experiment can help by providing direct measurements that are subject to smaller
81 uncertainty with finer spatial and temporal resolution albeit over limited ranges. The NASA
82 ObseRvations of Aerosols above CLouds and their intEractionS (ORACLES) mission was carried

83 out to study key processes that determine the climate impacts of African biomass-burning aerosols
84 above the southeast Atlantic. Of the two deployed aircraft, the NASA P3, equipped with in situ
85 and remote sensing instruments, flew in the lower- to mid-troposphere, mostly in September 2016,
86 August 2017 and October 2018. In September 2016 the NASA ER2 also flew, at about 20 km
87 altitude with downward-viewing sensors. Extensive stratocumulus clouds were observed
88 repeatedly throughout the mission; see a sample satellite image in Sayer et al. (2019). Details of
89 the ORACLES mission can be found in Redemann et al. (2020), Zuidema et al. (2016) and
90 Shinozuka et al. (2019).

91   The instrumentation relevant to the present paper is described in Sect. 2 along with
92 sampling and statistical hypothesis testing methods. This is followed by comparisons of AOD and
93 other aerosols properties above the height of cloud top between cloudy and clear skies (Sect. 3).
94 Sect. 4 offers discussion.

95 **2.   Methods**
96 **2.1.   Instrumentation**

97   The remote sensing and in situ instruments used in this study are briefly described below
98 with references to full descriptions. Note that the measurements each refer to a unique vertical
99 range, as summarized in Table 1.

100   The NASA Langley Research Center High Spectral Resolution Lidar (HSRL-2), deployed
101 from the ER2 in 2016 and from the P3 in 2017 and 2018, measures calibrated, unattenuated
102 backscatter and aerosol extinction profiles below the instrument. The data are reported with 10 s
103 intervals. The HSRL-2 S/N ratio is higher than that of CALIOP, due to the much lower altitude
104 and the inverse square dependence of light intensity. In addition, by the use of a second channel to
105 assess aerosol attenuation, the HSRL technique (Shipley et al., 1983) results in an accurate aerosol
106 extinction product with no assumptions about lidar ratio, and also a more accurate backscatter
107 product, particularly in the lower atmosphere where attenuation by upper layers can present
108 difficulties for the spaceborne backscatter lidar. Differences in algorithm are discussed in Sect. 4.
109 Further details about the instrument, calibration and uncertainty can be found in Hair et al. (2008),
110 Rogers et al. (2009) and Burton et al. (2018).

111   Our analysis utilizes the HSRL-2 standard products of cloud top height (CTH), 532 nm
112 particulate backscattering and 532 nm aerosol optical thickness (Burton et al., 2012) in three ways.

113   First, flight segments are isolated using the CTH product (detailed in Sect. 2.2). Second, the bottom

114   and top heights of the smoke plumes are defined with a (somewhat arbitrarily chosen) threshold

115   backscattering coefficient at 0.25 $Mm^{-1}sr^{-1}$ after Shinozuka et al. (2019).

116   Third, we evaluate the 532 nm partial-column aerosol optical thickness from below the

117   aircraft down to ~50 m above the CTH, (even for columns without clouds; see Sect. 2.2). The ~50-

118   m buffer is designed to reduce the ambiguity associated with the transition at the cloud top. The

119   upper limit of the integral of extinction is 14 km altitude for the 2016 ER2 flights and a certain

120   depth, 1500 m for most flights, below the P3 altitude for 2017 and 2018 (Fig. 1). Profiles with

121   possible influences of mid- and high-level clouds are largely excluded from the product, though

122   isolated cases of thin clouds may remain.

123   We also use partial-column AOD observed upward from the P3 with a sunphotometer (Fig.

124   1b,c). The Spectrometer for Sky-Scanning, Sun-Tracking Atmospheric Research (4STAR)

125   measures hyper-spectral direct solar beam. Calculated AOD is reported at 1 Hz. Our analysis

126   excludes data with possible influences of clouds above the instrument. Further details on the

127   instrument as well as data acquisition, screening, calibration and reduction can be found in

128   Dunagan et al. (2013), Shinozuka et al. (2013) and LeBlanc et al. (2019).

129   For 2017 and 2018, we examine a combination of the 4STAR and HSRL-2 AODs, in order

130   to cover the free troposphere both upward and downward from the aircraft that flew in it (Fig.

131   1b,c). The vertical coverage is compromised by two limitations intrinsic to the lidar measurements.

132   First, the CTH is not sought within 500 m of the instrument (not to be confused with the ~50-m

133   lower buffer for the extinction integral). This means that the flight segments with clouds so close

134   to the aircraft enter our analysis only if the clouds extended as deep as to reach 500 m away from

135   it. This is at most a minor fraction of the data, as the fraction with the CTH within 550 m of the P3

136   altitude is a mere 3%. Second, because of the 1500 m upper buffer for the P3-borne HSRL-2

137   extinction integral, we only have 4STAR above-P3 AOD for the flight segments when the plane

138   was 500-1500 m above the CTH (Fig. 1b). We add the HSRL-2 AOD to the 4STAR AOD only

139   for the flight segments when the P3 was >1500 m above the CTH (Fig. 1c).

140   For 2016, we examine the ER2-borne HSRL-2 AOD only, because, with the lidar above

141   the troposphere, two of the missing layers can safely be ignored, leaving the ~50 m lower buffer

142   as the only missing layer (Fig. 1a). We refer to all these AODs from the three campaigns

143   collectively as AOD_{ct} (see Table 1). The wavelength dependence expressed as Angstrom exponent

144   is calculated for 10-s periods with AOD_{ct} at 355 and 532 nm both exceeding 0.1.

145   In situ aerosol instruments operated from the P3 include a nephelometer (TSI model 3563)

146   and a particle soot absorption photometer (PSAP, Radiance Research 3-wavelength version),

147   which measure particulate light scattering and absorption, respectively. After adjustments are

148   made for factors such as angular truncations (Anderson and Ogren, 1998) and filter interference

149   (Virkkula, 2010) for each wavelength, extinction coefficient and single scattering albedo at 550

150   nm are derived for an instrument relative humidity (RH) that is typically below 40%. See Pistone

151   et al. (2019) and Shinozuka et al. (2019) for more details. The non-refractory masses of submicron

152   particles were measured by a time-of-flight aerosol mass spectrometer (Aerodyne, Inc HR-ToF

153   AMS, DeCarlo et al. (2006)). A condensation particle counter (TSI model 3010, with ΔT set to

154   22°C) measured the number concentration of particles larger than about 10 nm. These in situ

155   properties refer to the air immediately outside the P3 aircraft, not a vertical column. Only the in

156   situ measurements in 2017 and 2018 at 500-1500 m above the CTH are used in this study (Fig.

157   1b).

158   **2.2.   Sampling**

159   Two methods are employed for selecting subsets of the observations for analysis. In the

160   first (Sect. 2.2.1), we bundle data from areas hundreds of kilometers wide for each of the three

161   campaigns, in a manner as similar to the CALIOP-based study (Chung et al., 2016) as the airborne

162   measurements allow. In the second method (Sect. 2.2.2), we pair cloudy and clear skies with more

163   stringent spatiotemporal criteria to isolate the impact of finer-scale phenomena. Note that both

164   methods ignore time periods for which the 532 nm backscattering product (from which the CTH

165   product is derived) is masked at all altitudes, as well as transit flights into and out of the study area.

166   Cases are also excluded where the CTH exceeds 3241 m. This is to be consistent with the study

167   by Chung et al. (2016), which refers to clouds at 680 hPa or higher pressure, although we find

168   similar results with or without this restriction.

169   2.2.1.   **Meso-scale monthly-mean sampling**

170   This method separates profiles measured in the three campaigns into two groups: those

171   concurrent with a presence of low-level clouds as reported by the HSRL-2 and those concurrent

172 with an absence of any cloud detected by HSRL-2 in the column. The groups are each aggregated

173 into grid boxes approximately 2° by 2°, as shown in Fig. 2. This grid is adapted from Shinozuka et

174 al. (2019) but with additional boxes for the São Tomé-based 2017 and 2018 campaigns. In total,

175 109 hours and 39 hours of flight segments are selected for the cloudy and clear groups,

176 respectively, including minor double-counting where boxes overlap.

177   The arithmetic mean of the CTH of the cloudy group is calculated for each day for each

178 box and 50 m above it is set as the lowest altitude for computing AOD_{ct} for each 10 s period (Sect.

179 2.1). Then the arithmetic mean and standard deviation are calculated for the AOD_{ct}, as well as

180 other measurements (Sect. 2.1, Table 1), for each group and each box. We exclude the boxes with

181 fewer than 10 counts of 10-second averages and the time periods with mid- and high-level clouds

182 and instrument/aircraft issues. Forty-nine hours and twenty-six hours of the AOD_{ct} measurements

183 enter the analysis for cloudy and clear-sky groups, respectively.

184   2.2.2.   **Local-scale near-synchronous sampling**

185   This method identifies cloud edges and demarcates the cloudy side and clear side of each

186 edge based on the time series of the CTH detected by HSRL-2, for level flight legs only. Cloud

187 edges are defined by the points in time when a cloud is detected in a profile adjacent to a profile

188 with no cloud detection.

189   A clear sky and a cloud are represented by the time period of a certain length, 60 s in the

190 example illustrated in Fig. 3a, preceding each edge and the same length following it. To ensure

191 that clear skies and clouds are not interrupted for the length, we exclude edges for which another

192 one is found within the length. The longer the length, the smaller the number of cloudy-clear pairs,

193 because longer continuous clouds and clear skies are rarer. Furthermore, we set another length,

194 say 20 s, to exclude immediately before and after the edge, in order to reduce ambiguity associated

195 with a gradual transition from cloud droplets to unactivated particles, the so-called twilight zone

196 (Koren et al., 2007; Schwarz et al., 2017; Várnai and Marshak, 2018). We convert the temporal

197 dimensions into horizontal ones using the mean true horizontal aircraft speed, 200 ms^{-1} for the

198 ER2 (Fig. 3a) and 140 ms^{-1} for the P3 (Fig. 3b and Fig. 3c).

199   While Fig. 3a has one set of maximum and minimum limits of separation noted as an

200 example, we alter them in order to assess scale dependence and sampling error as much as our

201 airborne data permit. The way the edges are identified ensures that a measurement cannot be

202 counted more than twice for a given range of separation. A measurement can, however, enter
203 multiple ranges of separation. For example, a measurement 4-6 km away from a cloud edge enters
204 the ranges of 0-6 km, 2-6 km, 2-12 km, 4-12 km, 4-20 km, etc. In total, 5.0 hours of horizontal
205 flight are selected, including the double-counting for a given range but excluding the multiple-
206 counting over multiple ranges. Exactly half of them are over clouds. Note that these expressions
207 of separation are only notional; we discuss this in Sect. 4.

208   As with the meso-scale monthly-mean sampling, we take the arithmetic mean of the CTH
209 of the cloudy side and add 50 m (red lines in Fig. 3). The height is extended to the adjacent clear
210 sky (orange lines) for the calculation of AOD_{ct} (Sect. 2.1). The in situ measurements (Sect. 2.1,
211 Table 1) are each averaged over the cloudy sides and over the clear sides. Cases where aerosol
212 measurements are unavailable for 33% or more of the time period, for example due to calibration
213 or operation problems, are excluded. This makes the number of cloudy-clear pairs vary from
214 property to property for a given range of separation. In total, 3.8 hours of AOD_{ct} measurements
215 enter the analysis.

216 ### 2.3.   Statistical hypothesis testing

217   We employ the paired t-test, also called paired-samples t-test or dependent t-test, to
218 determine whether the mean difference in each property, x (e.g., AOD_{ct}), between the presence
219 and absence of low-level clouds is statistically consistent with the null hypothesis of zero
220 difference. The procedure entails calculating the t statistic, the ratio of the mean cloudy-clear
221 differences to their standard error, E.

222
$$t = \underline{\Delta x}/E$$

223
$$E = \sigma/\sqrt{N}$$

224 Here the standard error is the standard deviation computed for N-1 degrees of freedom, σ, divided
225 by the square root of N, where N is the number of sample pairs. Note that the standard deviation is
226 close to the root-mean-square deviation (RMSD) for small absolute mean difference, unless N is
227 smaller than five.

228   For the calculated t statistic, the two-tailed p value is looked up. Small p values are
229 associated with large t statistics and hence generally large mean differences relative to RMSD. If
230 the p value is smaller than 0.05, we reject the null hypothesis. If it is greater, we do not.

231   The procedure makes several assumptions. One is independence of the differences.
232   Synoptic- and meso-scale phenomena prevalent throughout ORACLES (e.g., subsidence and
233   anticyclones) reduce the independence of the samples. The low day-to-day meteorological
234   variability and repeated flight paths might mean that the same aerosol-cloud conditions were
235   sampled day after day. It is unclear whether this would reduce the independence of the cloudy-
236   clear differences - a potential, seemingly untestable caveat for the meso-scale monthly-mean
237   sampling (Sect. 2.2.1). In the local scale the exclusion of contiguous cloud edges (Sect. 2.2.2)
238   should attain a high level of independence from one another. The procedure also assumes
239   continuous (not discrete), approximately normally distributed data free of outliers.

240   **3.   Results**

241   The meso-scale monthly-mean method finds little systematic difference in 532 nm AOD_{ct}
242   (Fig. 4). Most markers lie near the 1:1 line. The mean difference, an indicator of systematic
243   differences, is +0.01. This is only +9% of the RMSD, an indicator of the total (random and
244   systematic) variability. The p value from the paired t-test is 0.54. Thus, the AOD above low-level
245   clouds is not significantly different from that at the same heights above nearby clear skies in this
246   scale. The p value is also greater than 0.05 for $\log_{10}$ of AOD_{ct}, something we tested just to confirm
247   that our conclusions do not depend on the choice of linear or log scale. The same goes for the
248   Angstrom exponent and in situ aerosol properties (Table 2, see the rows labeled "box means").
249   The only exception is the organic mass with a p value just under 0.05 (before rounding).

250   The local-scale near-synchronous method finds virtually the same results. The AOD_{ct} is
251   compared in Fig. 5a for 2-6 km separation. The time period corresponds to approximately 10-30 s
252   temporal range on the ER2 (13 data points from the 2016 campaign) and 14-43 s at the average P3
253   speed (53 from 2017 and 2018). All data points lie near the 1:1 line. The mean difference, -0.002,
254   is only -21% of the RMSD for 2-6 km separation. The p value is 0.08.

255   We run the same calculation for other combinations of minimum and maximum separation.
256   Fig. 6 shows the resulting statistics. The mean difference for 2-6 km separation, for example, is
257   represented in Fig. 6a at maximum separation (x axis) of 6 km by the solid orange line that starts
258   after the minimum separation of 2 km. This line also shows that the mean difference is -0.01 if the
259   maximum separation is set to 20 km while keeping the minimum at 2 km. The longest blue line
260   represents the calculations for zero minimum separation (i.e., with the twilight zone included). All

261   other solid lines represent the results with greater minimum separation. For example, the green
262   line that is missing data up to 4 km indicates that the mean difference is closer to -0.01 at 12 km,
263   as shown in Fig. 5b.

264   For the separation up to 20 km, the mean difference is mostly between 0 and -0.01. The p
265   value, shown in Fig. 6b, is below 0.05 for only a handful of the ranges of separation, most of
266   which, with minimum separation of 0-2 km, are subject to potential ambiguity associated with the
267   so-called twilight zone (Sect. 2.2.2). Given that a p-value of 0.05 simply means that there is a one
268   in 20 chance that the null hypothesis is correct, we expect some low p-values just by chance as we
269   conduct many comparisons. The scarcity of low p values is also evident for $\log_{10}$ of AOD_{ct}, the
270   Angstrom exponent and in situ aerosol properties including the organic mass (Table 2). Large p
271   values are also found for the ER2- and P3-borne measurements separately and for the 4STAR and
272   the HSRL-2 AOD separately for 2017 and 2018.

273   **4.   Discussion and conclusions**

274   Virtually no systematic differences in aerosol properties are found between the air above
275   low-level clouds and that above nearby clear areas in ORACLES daytime airborne measurements.
276   The finding holds for a range (0-20 km) of distances between, and expanses of, the two air masses.
277   Note that the temporal and horizontal dimensions associated with the local-scale near-synchronous
278   sampling must be collectively overestimated, because the aircraft may have been running parallel
279   to cloud edge. There is no easy way to know how far from the nearest cloud edge the airplane was
280   in reality. Images from cameras on the plane and satellites may give some context. But we stop
281   short of examining them, due to the perceived difficulty in unifying the definition of cloud edges
282   between the cameras and the lidar, among other image processing issues. Although we do not
283   know what the real distances and expanses are, that probably does not matter for the region and
284   season of our study, judging by the consistently large p values across the notional distances and
285   expanses. The meso-scale monthly-average sampling, resting on larger data, provides consistent
286   results. We note that this conclusion may or may not apply to environments elsewhere, especially
287   those with less uniform clouds.

288   Our analysis does not support aerosol-cloud interactions, circulation patterns or anything
289   else as a cause for a significant systematic difference in aerosol amounts, simply because such a
290   difference is not evident. The lack of obvious sensitivity to the smoke-cloud gap height, indicated

291   by marker color in Fig. 5, is consistent with this conclusion. The smoke bottom height minus the

292   mean CTH gives an estimate of whether aerosols may be physically in contact with clouds and

293   therefore there is a chance of wet removal and cloud processing. Our analysis does not detect any

294   sign of local aerosol removal by the underlying clouds.

295   An important difference between the present analysis and the CALIOP-based one (Chung

296   et al., 2016), apart from the spatiotemporal range and resolution, is that the HSRL algorithm does

297   not use any explicit layer detection (Hair et al., 2008). The return signal in the molecular signal

298   provides a measure of the aerosol attenuation and extinction. A very tenuous aerosol layer still

299   produces a reported extinction with a reported error bar. If the aerosol extinction is very small, the

300   error bar may exceed the retrieved value, but there is no cutoff at small values that produces the

301   kind of bias one gets from a detection threshold. Furthermore, the S/N ratio is higher than that of

302   CALIOP and no assumptions about lidar ratio are made, as explained in Sect. 2.1.

303   We posit that the systematic differences between above-cloud and clear skies AODs shown

304   in Chung et al. (2016) are *solely* a CALIOP retrieval artifact, at least for the ORACLES region and

305   season. As described in Sect. 1, the CALIOP standard algorithm has a detection bias that leads to

306   greater AOD underestimates over clouds than in clear skies by day due to upward sunlight

307   reflection. The authors emphasize that this bias might explain their results, pointing to a day-night

308   contrast as evidence: "a corresponding difference cannot be seen in the ΔAOD_{ct} derived from

309   nighttime retrievals [which are free of sunlight reflection]". The present study corroborates this

310   hypothesis, by rejecting the other possible explanations related to aerosol amounts.

311   We should note that the detection bias due to a low S/N ratio is not the only known source

312   of error in the daytime CALIOP standard AOD product. The error can also originate from a

313   misclassified aerosol type and, hence, an incorrectly assumed lidar ratio in the CALIOP algorithm.

314   Such an aerosol misclassification can either over- or under-estimate CALIOP AOD, unlike an

315   undetected aerosol layer. Misclassification and low S/N ratio, taken together, explain the absence

316   of a significant bias between CALIOP and HSRL-1 above-cloud AODs in a low aerosol-above-

317   cloud environment such as over Northern America in Kacenelenbogen et al. (2014). On the other

318   hand, Liu et al. (2015) describe a CALIOP standard daytime AOD underestimate above clouds

319   over two regions of high above-cloud AODs. While both misclassification and low S/N ratio are

320   at play, Liu et al. (2015) mainly explain the CALIOP above-cloud AOD underestimate by a low

321   S/N ratio (especially when solar light is reflected on the underlying cloud) in the case of smoke in

322 South East Atlantic, and an underestimate of the lidar ratio in the case of Saharan dust (see their
323 Table 2).

324   In Chung et al. (2016), the lower daytime CALIOP AOD above clouds can be explained
325 mainly by CALIOP's low S/N ratio as there is no reason to believe that CALIOP would show a
326 different classification bias above clouds compared to nearby clear skies. The depolarization ratio
327 method by Hu et al. (2007) retrieves above-cloud AOD from CALIOP without a layer detection
328 algorithm. This method may lead to a different result from Chung et al. (2016). A future study
329 based on the Hu et al. (2007) method and extended to the globe as in Kacenelenbogen et al. (2019)
330 will also address environments under a wider variety of synoptic- and meso-scale conditions that
331 produce specific opaque water clouds.

332   Going back to the present aircraft-based study, the absence of systematic differences is
333 good news, because satellite retrievals and studies of radiative effects do not need to treat these
334 two conditions as different. Our results on AOD_{ct} justify, for example, temporal and horizontal
335 extrapolation of above-cloud AOD to adjacent clear skies and attribution of the difference from
336 full-column AOD to the planetary boundary layer. Our results on the aerosol intensive properties
337 suggest that a single set of aerosol models can be used for the aerosols in the free troposphere
338 regardless of whether clouds exist below, which may allow better characterization of the
339 underlying clouds and the radiative effects (Matus et al., 2015; Meyer et al., 2015). It seems
340 reasonable to use aerosol properties retrieved in clear skies for estimating the direct radiative
341 effects of aerosols above nearby clouds, as in Kacenelenbogen et al. (2019). But challenges remain.
342 Random variability in AOD and other aerosol properties is significant, as indicated by RMSD in
343 the present study and quantified for smoke elsewhere (Shinozuka and Redemann, 2011). It may
344 be problematic to assume the same values for intensive properties for reasons not investigated
345 here, for example: form of combustion, degree of aerosol ageing and influence of the boundary
346 layer. These may be tackled more effectively by combining sensors of various capabilities with
347 improved spatiotemporal resolution and retrieval algorithms (National Academies of Sciences,
348 Engineering, and Medicine, 2018). These improved satellite observations of aerosol properties in
349 clear skies and above clouds are urgently needed to reduce the uncertainty in total aerosol radiative
350 forcing. For this, we are looking forward to the next generation of space-borne lidars, radars,
351 microwave radiometers, polarimeters and spectrometers such as the ones that will address joint

352 Aerosols, Clouds, Convection and Precipitation (ACCP) science goals and objectives
353 (https://science.nasa.gov/earth-science/decadal-accp)

354 **Data availability**

355   The P3 and ER2 observational data (ORACLES Science Team, 2020a, 2020b, 2020c) are
356 available   through   http://dx.doi.org/10.5067/Suborbital/ORACLES/ER2/2016_V2,
357 http://dx.doi.org/10.5067/Suborbital/ORACLES/P3/2017_V2   and
358 doi:10.5067/Suborbital/ORACLES/P3/2018_V2.

359 **Author contribution**

360   All authors participated in the investigation during the ORACLES intensive observation
361 periods. In addition, MSK led conceptualization, funding acquisition, methodology, project
362 administration and supervision. YS led data curation, formal analysis, software and validation and
363 wrote the original draft. YS and MSK contributed visualization. All but CJF reviewed and edited
364 the manuscript.

365   **Competing interests**

366   The authors declare that they have no conflict of interest.

367   **Acknowledgments**

368   We would like to thank Eric Wilcox and one anonymous referee for reading the manuscript
369 and providing valuable comments. In addition, we thank Tamás Várnai and Sasha Marshak for
370 discussion. ORACLES is funded by NASA Earth Venture Suborbital-2 grant NNH13ZDA001N-
371 EVS2. We would like to thank the personnel and crews of the NASA P3 and ER2 for their help in
372 collecting the datasets.

373   **References**

374 Anderson, T. L. and Ogren, J. A.: Determining aerosol radiative properties using the TSI 3563 integrating
375 nephelometer, Aerosol Sci. Technol., 29, 57–69, 1998.

376 Burton, S. P., Ferrare, R. A., Hostetler, C. A., Hair, J. W., Rogers, R. R., Obland, M. D., Butler, C. F.,
377 Cook, A. L., Harper, D. B. and Froyd, K. D.: Aerosol classification using airborne High Spectral
378 Resolution Lidar measurements – methodology and examples, Atmospheric Measurement Techniques,
379 5(1), 73–98, 2012.

380 Burton, S. P., Hostetler, C. A., Cook, A. L., Hair, J. W., Seaman, S. T., Scola, S., Harper, D. B., Smith, J.
381 A., Fenn, M. A., Ferrare, R. A., Saide, P. E., Chemyakin, E. V. and Müller, D.: Calibration of a high
382 spectral resolution lidar using a Michelson interferometer, with data examples from ORACLES, Appl.
383 Opt., 57(21), 6061–6075, 2018.

384 Chung, C. E., Lewinschal, A. and Wilcox, E.: Relationship between low-cloud presence and the amount
385 of overlying aerosols, Atmos. Chem. Phys., 16(9), 5781–5792, 2016.

386 Costantino, L. and Bréon, F.-M.: Analysis of aerosol-cloud interaction from multi-sensor satellite
387 observations, Geophys. Res. Lett., 37(11), doi:10.1029/2009gl041828, 2010.

388 Costantino, L. and Bréon, F.-M.: Aerosol indirect effect on warm clouds over South-East Atlantic, from
389 co-located MODIS and CALIPSO observations, Atmos. Chem. Phys., 13(1), 69–88, 2013.

390 DeCarlo, P. F., Kimmel, J. R., Trimborn, A., Northway, M. J., Jayne, J. T., Aiken, A. C., Gonin, M.,
391 Fuhrer, K., Horvath, T., Docherty, K. S., Worsnop, D. R. and Jimenez, J. L.: Field-Deployable, High-
392 Resolution, Time-of-Flight Aerosol Mass Spectrometer, Anal. Chem., 78(24), 8281–8289, 2006.

393 Dunagan, S. E., Johnson, R., Zavaleta, J., Russell, P. B., Schmid, B., Flynn, C., Redemann, J., Shinozuka,
394 Y., Livingston, J. and Segal-Rosenhaimer, M.: Spectrometer for Sky-Scanning Sun-Tracking
395 Atmospheric Research (4STAR): Instrument Technology, Remote Sensing, 5(8), 3872–3895, 2013.

396 Hair, J. W., Hostetler, C. A., Cook, A. L., Harper, D. B., Ferrare, R. A., Mack, T. L., Welch, W.,
397 Izquierdo, L. R. and Hovis, F. E.: Airborne High Spectral Resolution Lidar for profiling aerosol optical
398 properties, Appl. Opt., 47(36), 6734–6752, 2008.

399 Hu, Y., Vaughan, M., Liu, Z., Powell, K. and Rodier, S.: Retrieving Optical Depths and Lidar Ratios for
400 Transparent Layers Above Opaque Water Clouds From CALIPSO Lidar Measurements, IEEE
401 Geoscience and Remote Sensing Letters, 4(4), 523–526, 2007.

402 Johnson, B. T., Shine, K. P. and Forster, P. M.: The semi-direct aerosol effect: Impact of absorbing
403 aerosols on marine stratocumulus, Quarterly Journal of the Royal Meteorological Society, 130(599),
404 1407–1422, doi:10.1256/qj.03.61, 2004.

405 Kacenelenbogen, M., Redemann, J., Vaughan, M. A., Omar, A. H., Russell, P. B., Burton, S., Rogers, R.
406 R., Ferrare, R. A. and Hostetler, C. A.: An evaluation of CALIOP/CALIPSO's aerosol-above-cloud
407 detection and retrieval capability over North America, J. Geophys. Res. D: Atmos., 119(1), 230–244,
408 2014.

409 Kacenelenbogen, M. S., Vaughan, M. A., Redemann, J., Young, S. A., Liu, Z., Hu, Y., Omar, A. H.,
410 LeBlanc, S., Shinozuka, Y., Livingston, J. and Others: Estimations of global shortwave direct aerosol
411 radiative effects above opaque water clouds using a combination of A-Train satellite sensors, Atmos.
412 Chem. Phys., 19(7), 4933–4962, 2019.

413 Koren, I., Remer, L. A., Kaufman, Y. J., Rudich, Y. and Vanderlei Martins, J.: On the twilight zone
414 between clouds and aerosols, Geophysical Research Letters, 34(8), doi:10.1029/2007gl029253, 2007.

415 LeBlanc, S. E., Redemann, J., Flynn, C., Pistone, K., Kacenelenbogen, M., Segal-Rosenheimer, M.,
416 Shinozuka, Y., Dunagan, S., Dahlgren, R. P., Meyer, K., Podolske, J., Howell, S. G., Freitag, S., Small-
417 Griswold, J., Holben, B., Diamond, M., Formenti, P., Piketh, S., Maggs-Kölling, G., Gerber, M. and
418 Namwoonde, A.: Above Cloud Aerosol Optical Depth from airborne observations in the South-East
419 Atlantic, , doi:10.5194/acp-2019-43, 2019.

420 Matus, A. V., L'Ecuyer, T. S., Kay, J. E., Hannay, C. and Lamarque, J.-F.: The Role of Clouds in
421 Modulating Global Aerosol Direct Radiative Effects in Spaceborne Active Observations and the
422 Community Earth System Model, J. Clim., 28(8), 2986–3003, 2015.

423 Meyer, K., Platnick, S. and Zhang, Z.: Simultaneously inferring above-cloud absorbing aerosol optical
424 thickness and underlying liquid phase cloud optical and microphysical properties using MODIS, J.
425 Geophys. Res. D: Atmos., 120(11), 5524–5547, 2015.

426 National Academies of Sciences, Engineering, and Medicine: Thriving on Our Changing Planet: A
427 Decadal Strategy for Earth Observation from Space, The National Academies Press, Washington, DC.,
428 2018.

429 ORACLES Science Team: Suite of Aerosol, Cloud, and Related Data Acquired Aboard ER2 During
430 ORACLES 2016, Version 2, doi:10.5067/Suborbital/ORACLES/ER2/2016_V2, 2020a.

431 ORACLES Science Team: Suite of Aerosol, Cloud, and Related Data Acquired Aboard P3 During
432 ORACLES 2017, Version 2, doi:10.5067/Suborbital/ORACLES/P3/2017_V2, 2020b.

433 ORACLES Science Team: Suite of Aerosol, Cloud, and Related Data Acquired Aboard P3 During
434 ORACLES 2018, Version 2, doi:10.5067/Suborbital/ORACLES/P3/2018_V2, 2020c.

435 Pistone, K., Redemann, J., Doherty, S., Zuidema, P., Burton, S., Cairns, B., Cochrane, S., Ferrare, R.,
436 Flynn, C., Freitag, S., Howell, S. G., Kacenelenbogen, M., LeBlanc, S., Liu, X., Schmidt, K. S., Sedlacek,
437 A. J., III, Segal-Rozenhaimer, M., Shinozuka, Y., Stamnes, S., van Diedenhoven, B., Van Harten, G. and
438 Xu, F.: Intercomparison of biomass burning aerosol optical properties from in situ and remote-sensing
439 instruments in ORACLES-2016, Atmos. Chem. Phys., 19(14), 9181–9208, 2019.

440 Redemann, Wood, Zuidema, Doherty, Luna, LeBlanc, Diamond, Shinozuka, Ueyama, Pfister, DaSilva,
441 Longo, Kacenelenbogen, Knox, Piketh, Haywood, Formenti, Mallet, Stier, Ackerman, Carmichael, Saide,
442 Howell, Cairns, Knobelspiesse, Tanelli, L'Ecuyer, McFarquhar, Poellot, Nenes, Kacarab, Pui Shan
443 Wong, Small-Griswold, Thornhill, Noone, Podolske, Schmidt, Sedlacek, Lang, Stith, Segal-Rozenhaimer,
444 Hostetler, Ferrare, Burton, Diner, Platnick, Myers, Meyer, Spangenberg, Ian Chang: An overview of the
445 ORACLES (ObseRvations of Aerosols above CLouds and their intEractionS) project: aerosol-cloud-
446 radiation interactions in the Southeast Atlantic basin, n.d.

447 Rogers, R. R., Hair, J. W., Hostetler, C. A., Ferrare, R. A., Obland, M. D., Cook, A. L., Harper, D. B.,
448 Burton, S. P., Shinozuka, Y., McNaughton, C. S., Clarke, A. D., Redemann, J., Russell, P. B., Livingston,
449 J. M. and Kleinman, L. I.: NASA LaRC airborne high spectral resolution lidar aerosol measurements
450 during MILAGRO: observations and validation, Atmos. Chem. Phys., 9(14), 4811–4826, 2009.

451 Sayer, A. M., Hsu, N. C., Lee, J., Kim, W. V., Burton, S., Fenn, M. A., Ferrare, R. A., Kacenelenbogen,
452 M., LeBlanc, S., Pistone, K., Redemann, J., Segal-Rozenhaimer, M., Shinozuka, Y. and Tsay, S.-C.: Two
453 Decades Observing Smoke Above Clouds in the South-Eastern Atlantic Ocean: Deep Blue Algorithm
454 Updates and Validation with ORACLES Field Campaign Data, [online] Available from:
455 https://ntrs.nasa.gov/search.jsp?R=20190028671 (Accessed 5 June 2020), 2019.

456 Schwarz, K., Cermak, J., Fuchs, J. and Andersen, H.: Mapping the Twilight Zone—What We Are
457 Missing between Clouds and Aerosols, Remote Sensing, 9(6), 577, 2017.

458 Shinozuka, Y. and Redemann, J.: Horizontal variability of aerosol optical depth observed during the
459 ARCTAS airborne experiment, Atmos. Chem. Phys., 11(16), 8489–8495, 2011.

460 Shinozuka, Y., Johnson, R. R., Flynn, C. J., Russell, P. B., Schmid, B., Redemann, J., Dunagan, S. E.,
461 Kluzek, C. D., Hubbe, J. M., Segal-Rosenheimer, M., Livingston, J. M., Eck, T. F., Wagener, R.,
462 Gregory, L., Chand, D., Berg, L. K., Rogers, R. R., Ferrare, R. A., Hair, J. W., Hostetler, C. A. and
463 Burton, S. P.: Hyperspectral aerosol optical depths from TCAP flights, J. Geophys. Res. D: Atmos.,
464 2013JD020596, 2013.

465 Shinozuka, Y., Saide, P. E., Ferrada, G. A., Burton, S. P., Ferrare, R., Doherty, S. J., Gordon, H., Longo,
466 K., Mallet, M., Feng, Y., Wang, Q., Cheng, Y., Dobracki, A., Freitag, S., Howell, S. G., LeBlanc, S.,
467 Flynn, C., Segal-Rosenhaimer, M., Pistone, K., Podolske, J. R., Stith, E. J., Bennett, J. R., Carmichael, G.
468 R., da Silva, A., Govindaraju, R., Leung, R., Zhang, Y., Pfister, L., Ryoo, J.-M., Redemann, J., Wood, R.
469 and Zuidema, P.: Modeling the smoky troposphere of the southeast Atlantic: a comparison to ORACLES
470 airborne observations from September of 2016, Aerosols/Field Measurements/Troposphere/Chemistry
471 (chemical composition and reactions), doi:10.5194/acp-2019-678, 2019.

472 Shipley, S. T., Tracy, D. H., Eloranta, E. W., Trauger, J. T., Sroga, J. T., Roesler, F. L. and Weinman, J.
473 A.: High spectral resolution lidar to measure optical scattering properties of atmospheric aerosols. 1:
474 Theory and instrumentation, Appl. Opt., AO, 22(23), 3716–3724, 1983.

475 Stier, P., Schutgens, N. A. J., Bellouin, N., Bian, H., Boucher, O., Chin, M., Ghan, S., Huneeus, N.,
476 Kinne, S., Lin, G., Ma, X., Myhre, G., Penner, J. E., Randles, C. A., Samset, B., Schulz, M., Takemura,
477 T., Yu, F., Yu, H. and Zhou, C.: Host model uncertainties in aerosol radiative forcing estimates: results
478 from the AeroCom Prescribed intercomparison study, Atmos. Chem. Phys., 13(6), 3245–3270, 2013.

479 Várnai, T. and Marshak, A.: Satellite Observations of Cloud-Related Variations in Aerosol Properties,
480 Atmosphere, 9(11), 430, doi:10.3390/atmos9110430, 2018.

481 Virkkula, A.: Correction of the Calibration of the 3-wavelength Particle Soot Absorption Photometer (3λ
482 PSAP), Aerosol Sci. Technol., 44(8), 706–712, 2010.

483 Waquet, F., Peers, F., Ducos, F., Goloub, P., Platnick, S., Riedi, J., Tanré, D. and Thieuleux, F.: Global
484 analysis of aerosol properties above clouds, Geophys. Res. Lett., 40(21), 5809–5814, 2013.

485 Wilcox, E. M.: Stratocumulus cloud thickening beneath layers of absorbing smoke aerosol, Atmos. Chem.
486 Phys., 10(23), 11769–11777, 2010.

487 Winker, D. M., Vaughan, M. A., Omar, A., Hu, Y., Powell, K. A., Liu, Z., Hunt, W. H. and Young, S. A.:
488 Overview of the CALIPSO Mission and CALIOP Data Processing Algorithms, J. Atmos. Ocean.
489 Technol., 26(11), 2310–2323, 2009.

490 Zuidema, P., Redemann, J., Haywood, J., Wood, R., Piketh, S., Hipondoka, M. and Formenti, P.: Smoke
491 and clouds above the southeast Atlantic: Upcoming field campaigns probe absorbing aerosol's impact on
492 climate, Bull. Am. Meteorol. Soc., 97(7), 1131–1135, 2016.

493

494 **Table 1. Properties and instruments used in this study and the altitudes they refer to.**

Property	September 2016 on the ER2 aircraft		August 2017 and October 2018* on the P3 aircraft	
	Instrument	Altitude	Instrument	Altitude
cloud top height (CTH)	HSRL-2	Limited to ≤3241 m in this study	HSRL-2	No higher than 500 m below the P3 and ≤3241 m
aerosol optical depth above cloud top height (AOD$_{ct}$)	HSRL-2	from ~50 m above the CTH to 14 km	4STAR	from the P3 to top of atmosphere (TOA), when the P3 is 500-1500 m above CTH
			HSRL-2 and 4STAR	from ~50 m above the CTH to TOA, except 0-1500 m below the P3, when the P3 is >1500 m above CTH
extinction coefficient, single scattering albedo, submicron non-refractory organic mass, number concentration	-	-	nephelometer, PSAP, HR-ToF AMS and condensation particle counter	at the P3 when the P3 is 500-1500 m above CTH

495   * One day in September 2017 and two days in September 2018 are also included.

496   - Not presented in this study. Observations were made from the P3, away from the ER2 for most

497   cases.

498

499

500

501 **Table 2. The mean values and the statistics on the cloudy-clear differences**

Sampling*	Mean	Mean Difference	RMSD	p	Number of Pairs
532 nm AOD_{ct}					
2-6 km	0.34	-0.00	0.01	0.08	66
4-12 km	0.34	-0.01	0.02	0.23	18
box means	0.28	+0.01	0.10	0.54	46
$\log_{10}$ 532 nm AOD_{ct}					
2-6 km	-0.53	-0.00	0.01	0.15	66
4-12 km	-0.53	-0.00	0.02	0.27	18
box means	-0.68	+0.03	0.18	0.21	46
Angstrom Exponent of AOD_{ct}					
2-6 km	1.19	-0.04	0.11	0.00	53
4-12 km	1.30	-0.02	0.05	0.08	16
box means	1.13	-0.01	0.10	0.63	43
In Situ 550 nm Extinction Coefficient (Mm^{-1})					
2-6 km	67.0	-0.2	3.0	0.87	7
4-12 km	84.6	-3.6	5.1	0.31	3
box means	64.1	+14.6	71.8	0.38	20
In Situ 550 nm Single Scattering Albedo					
2-6 km	0.85	-0.00	0.01	0.14	7
4-12 km	0.87	-0.01	0.01	0.35	3
box means	0.84	+0.01	0.05	0.57	20

Submicron Non-refractory Aerosol Organic Mass ($\mu g\ m^{-3}$)					
2-6 km	6.5	+0.1	0.5	0.75	9
4-12 km	6.1	-0.4	0.6	0.38	3
box means	7.0	+1.9	4.5	0.05	22
Number Concentration of Particles >10 nm (cm^{-3})					
2-6 km	1903	+5	59	0.82	10
4-12 km	2378	-110	121	0.09	3
box means	1574	+239	962	0.17	22

502   * Either the separation from cloud edges or box means.

503
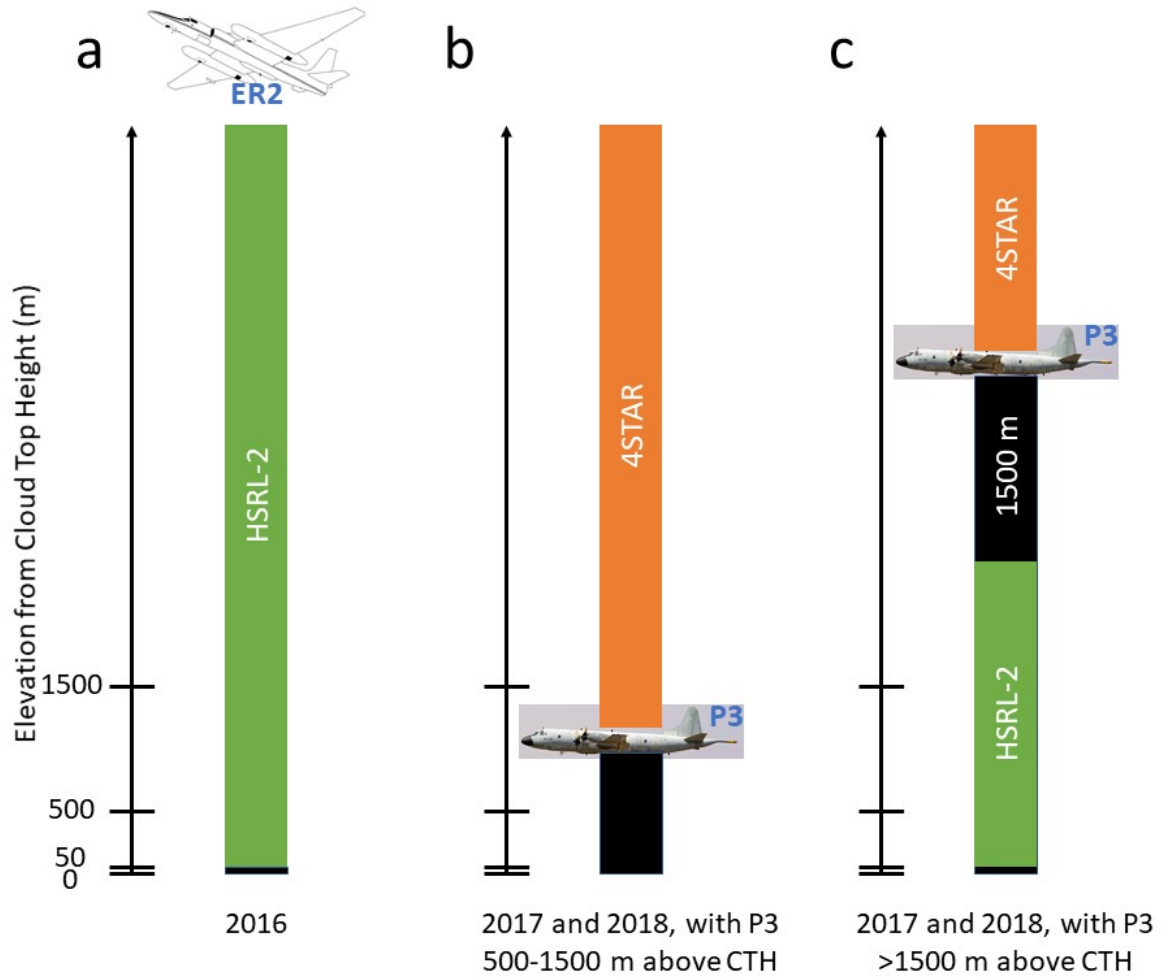
504

505   **Figure 1. AOD above cloud top height (AOD$_{ct}$). See text and Table 1 for details.**

506

507
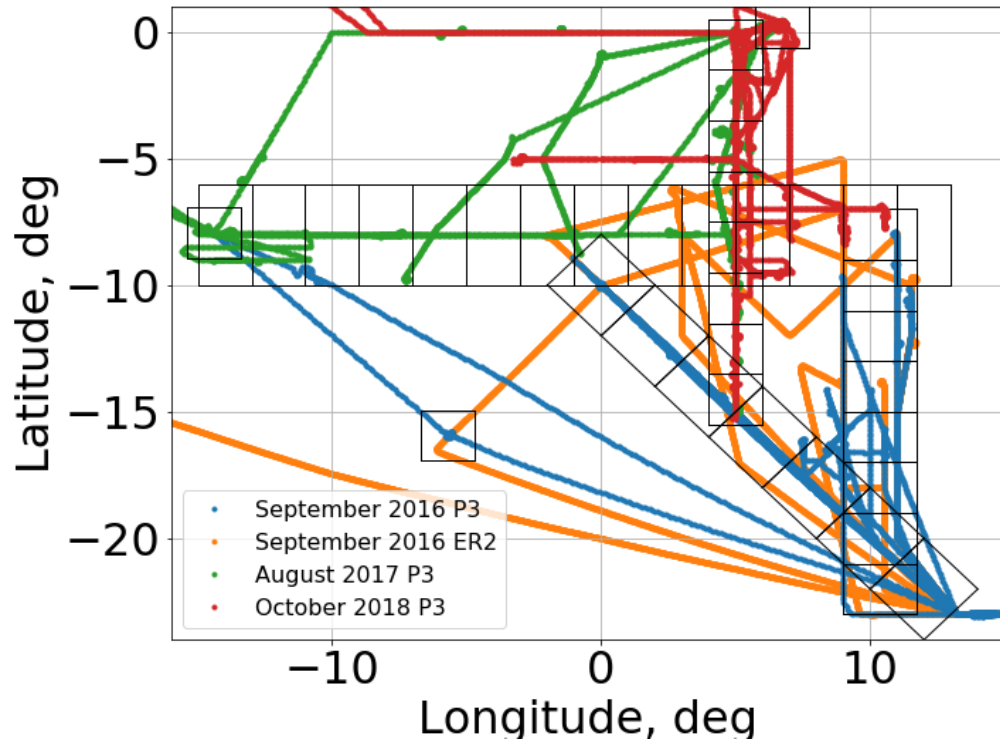
Figure 2. The flight paths of ORACLES. The boxes for meso-scale monthly-mean sampling are superimposed.

510

511

512

513

514

515
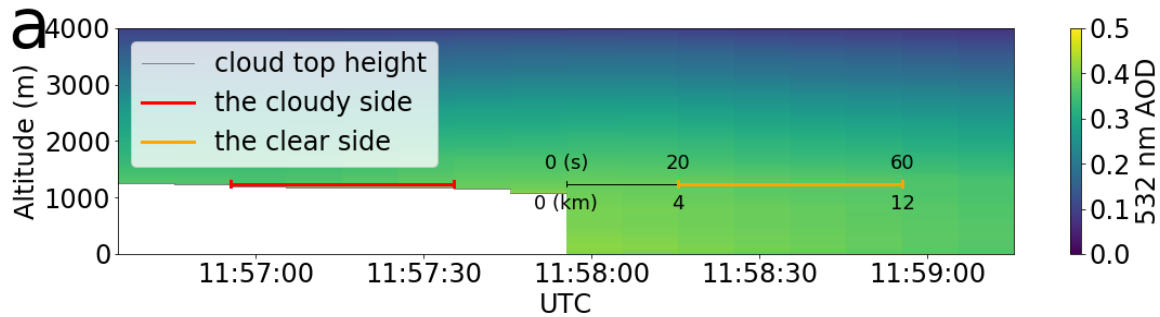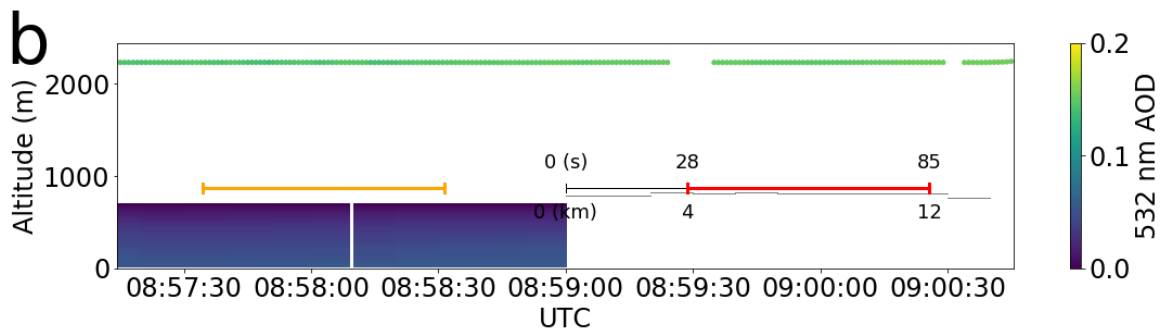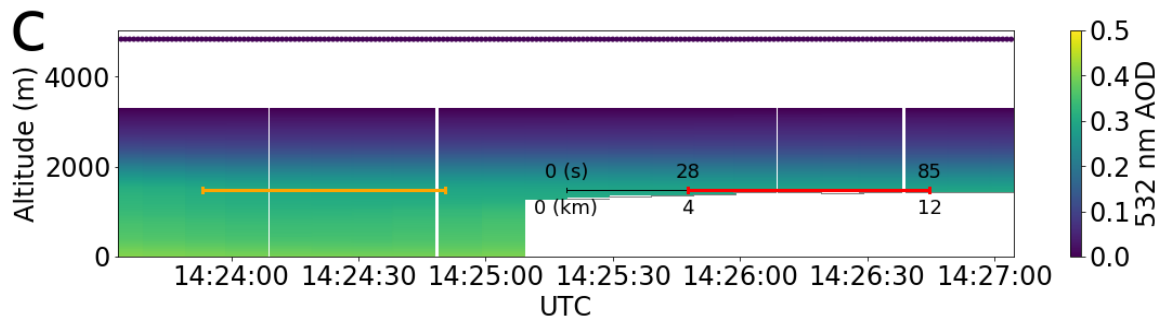
Figure 3. Examples of local-scale near-synchronous sampling, based on the HSRL-2 cloud top height (CTH) product; (a) In this subset of the ER2 flight on September 12, 2016, a cloud edge is found at 11:57:56 (denoted by 0 s and 0 km). The cloudy and clear side, each with horizontal separation of 4-12 km measured from cloud edge, are marked by red and orange lines, respectively. The HSRL-2 AOD profiles are given for altitudes from ~50 m above the clouds (as in Fig. 1a). (b) With the P3 500-1500 m above the CTH (Fig. 1b), as is the case with this example from October 5, 2018, we use 4STAR AOD only. The 4STAR AOD is indicated at the P3 altitudes just above 2000 m but refers to all altitudes above them. (c) With the P3 aircraft >1500 m above the CTH (Fig. 1c), as is the case for this example from August 12, 2017, the 4STAR AOD, indicated at the P3 altitudes just under 5000 m, is added to the HSRL-2 AOD at ~50 m above the CTH. The upper limit of the integral of extinction is 1500 m below the P3 altitude.

528

529

530

531
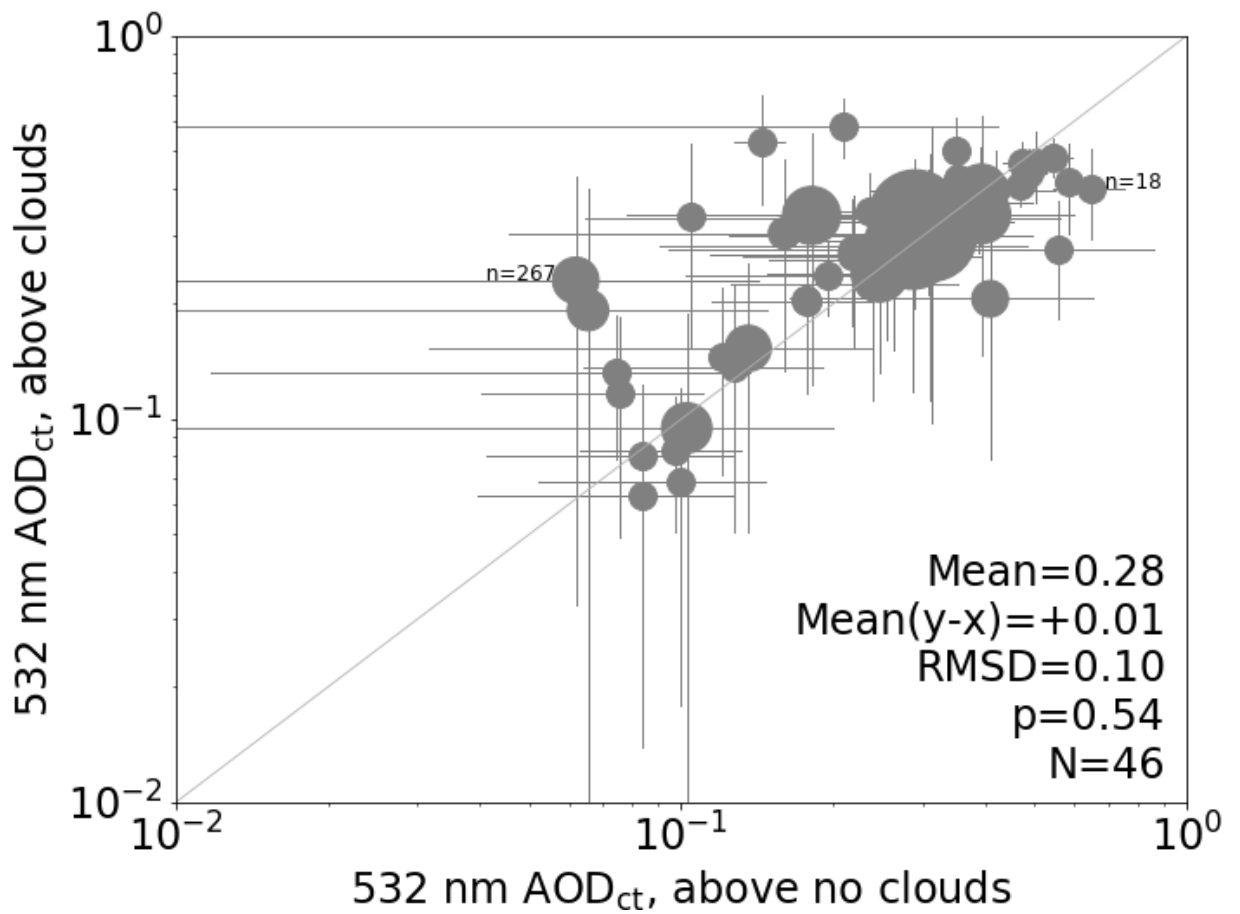
Figure 4. The meso-scale monthly-mean samples of the AOD above cloud top height. Each marker represents the mean over a box shown in Fig. 2. The bar represents the ±1 standard deviation range. The marker size is proportional to the number (n) of 10 s measurements for each combination of box and month, the fewer of the cloudy and clear groups. N refers to the number of monthly-box-means with n≥10 on both cloudy and clear cases.

538

539

540

541
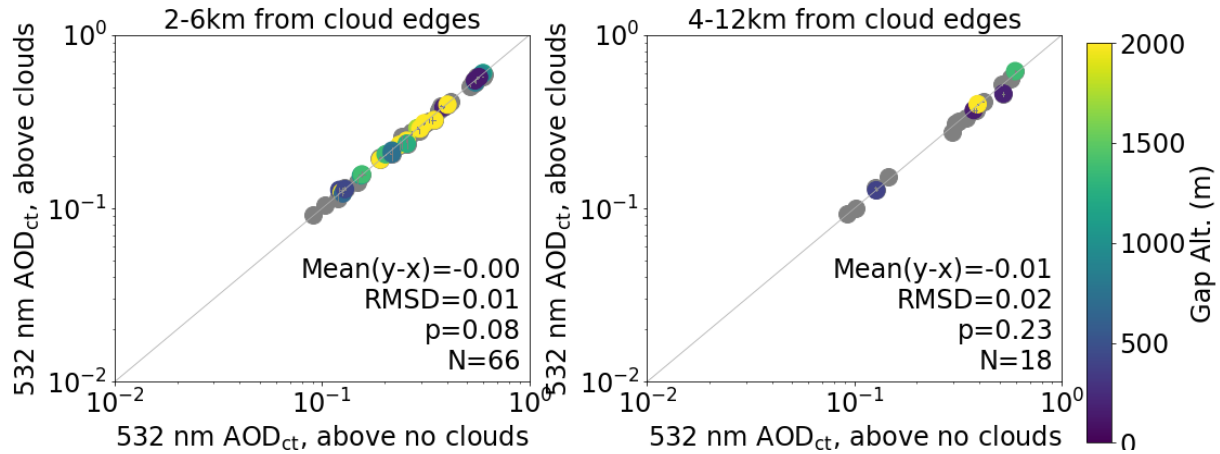
542
543 **Figure 5. (a) The local-scale near-synchronous samples of the AOD above cloud top height.**
544 **Each marker represents the mean over the cloudy and clear sides of a cloud edge, each 2-6**
545 **km from the edge. The bars indicate the standard deviation of the measurements in each**
546 **side, almost all of them too short to be discernible. (b) Same as (a) except for the horizontal**
547 **separation of 4-12 km.**

548

549

550

551
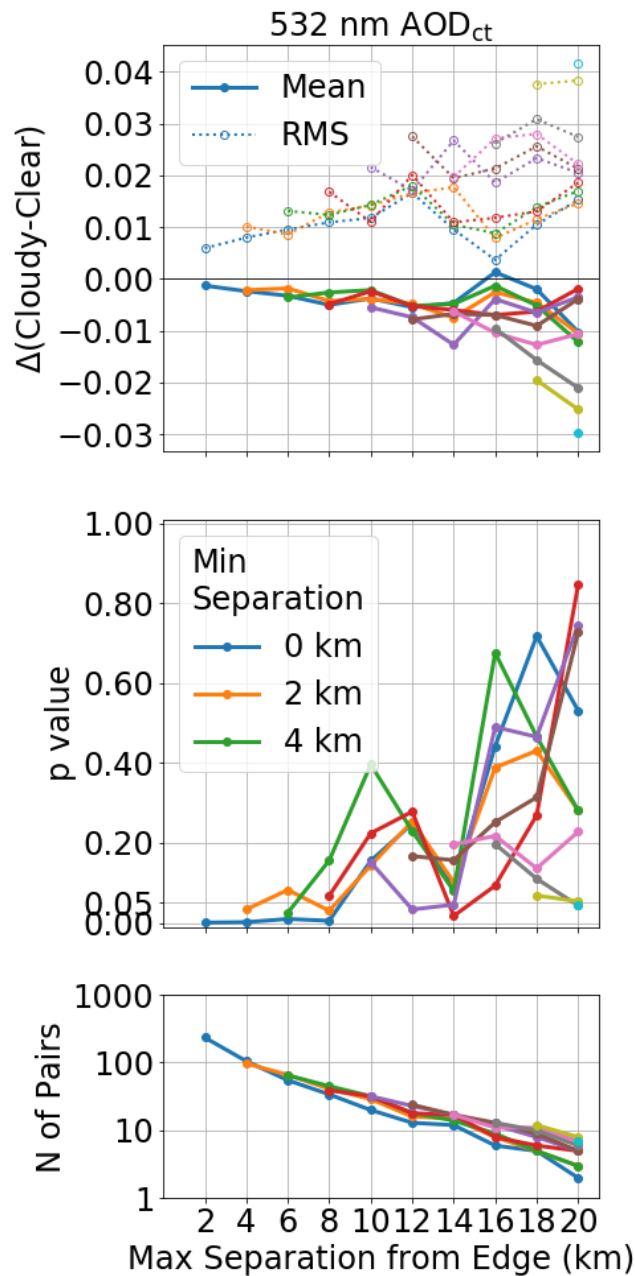
Figure 6. (a) The mean and root-mean-square deviations of the AOD above cloud top between the cloudy and clear sides of cloud edges. Each side is defined by the horizontal separation from cloud edge. The maximum separation (e.g., 12 km in Fig. 3) is indicated on the x axis. Each line represents the minimum temporal separation (e.g., 4 km in Fig. 3) of 0, 2, 4, …, 18 km in descending order of line length. (b) The p values determined through the paired t-test. (c) the number of cloudy/clear pairs.